THE ELECTRONIC STRUCTURE OF Fe^{2+} IN REACTION CENTERS FROM *RHODOPSEUDOMONAS SPHAEROIDES*

I. STATIC MAGNETIZATION MEASUREMENTS

W. F. BUTLER, D. C. JOHNSTON, H. B. SHORE, D. R. FREDKIN, M. Y. OKAMURA, AND G. FEHER, *Department of Physics, University of California, San Diego, La Jolla, California 92093 U.S.A.*

ABSTRACT We have measured the static magnetization of unreduced and reduced reaction centers that vary in their quinone content. Measurements were performed in the temperature range $0.7°K < T < 200°K$ and magnetic fields of up to 10 kG. The electronic g-value, crystal field parameters D, E, and the exchange interaction, J, between the quinone spin and Fe^{2+} were determined using the spin Hamiltonian formalism. The effective moment μ_{eff}/Fe^{2+} of both reduced and unreduced samples was determined to be 5.35 ± 0.15 Bohr magnetons. This shows, in agreement with previous findings, that Fe^{2+} does not change its valence state when the reaction centers are reduced. Typical values of $D \simeq +5$ cm^{-1} and $E/D \simeq 0.27$ are consistent with Fe being in an octahedral environment with rhombic distortion. The values of D and E were approximately the same for reaction centers having one and two quinones. These findings imply that quinone is most likely not a ligand of Fe. The Fe^{2+} and the spin on the quinone in reduced reaction centers were found to be coupled with an exchange interaction $0 < |J| < 1$ cm^{-1}. The validity of the spin Hamiltonian was checked by using an orbital Hamiltonian to calculate energy levels of the 25 states of the $S = 2$, $L = 2$ manifold and comparing the magnetization of the lowest five states with those obtained from the spin Hamiltonian. Using the orbital Hamiltonian, we calculated the position of the first excited quintet state to be 340 cm^{-1} above the ground state quintet. This is in good agreement with the temperature dependence of the quadrupole splitting as determined by Mossbauer spectroscopy.

INTRODUCTION

The primary process of bacterial photosynthesis involves the light-induced electron transfer from a primary electron donor to a sequence of electron acceptors. This is accomplished in a bacteriochlorophyll-protein complex called the reaction center (RC) which contains four bacteriochlorophylls, two bacteriopheophytins, two quinones, and one iron (for a comprehensive review, see Clayton and Sistrom, 1978). The primary donor is a bacteriochlorophyll dimer which, in the primary photochemistry, transfers its electron via bacteriopheophytin to the primary quinone Q_1. From Q_1 the electron passes to the secondary quinone Q_2. Electron

---

Dr. Johnston's present address is the Exxon Research and Engineering Corp., Linden, N.J. 07036.
Dr. Shore's present address is the Department of Physics, San Diego State University, San Diego, Calif. 92182.
Please address reprint requests to G. Feher.

paramagnetic resonance (EPR) experiments have shown that both Q_1 and Q_2 are magnetically coupled to the Fe (Wraight, 1978 *a*, and *b*, Okamura et al., 1978); these coupled complexes constitute the primary and secondary acceptors, respectively. The two Qs are distinguishable by their ease of removal with the detergent, lauryldimethylamine oxide (LDAO), and orthophenanthroline. The more easily removed Q_2 is not required for the primary photochemistry while the more tightly bound Q_1 plays an obligatory role in the primary acceptor (Okamura et al., 1975).

Removal of Fe does not abolish the primary photochemistry (Loach and Hall, 1972; Feher et al., 1972). Furthermore, it was shown by Mossbauer spectroscopy that the valence of Fe is +2 and remains unchanged when the acceptor is chemically reduced (Debrunner et al., 1975; Feher and Okamura, 1978). These experiments provide strong evidence that Fe is not directly involved in the primary photochemistry. It has been postulated that the function of the Fe is to facilitate the electron transfer from Q_1 to Q_2 (Okamura et al., 1975). Recent experiments by Blankenship and Parson (1979) support this hypothesis.

To understand the role of Fe in the electron transfer process, we have undertaken a study of its electronic structure and its interaction with the quinones. There are many physical techniques that can be brought to bear on this problem, e.g., optical spectroscopy, Mossbauer spectroscopy, extended x-ray fine structure (EXAFS), etc., some of which will be discussed in later publications. In this work, we report on the magnetic properties of the ground state of iron in both reduced and unreduced RCs. EPR, whenever applicable, is usually the method of choice for investigating the magnetic properties of transition metals. Unfortunately, iron in RCs has an even number of electrons. Consequently, the ground state cannot have a Kramers degeneracy; this makes it difficult to observe an EPR signal by conventional methods (Abragam and Bleaney, 1970). We therefore determined the magnetization of iron by static magnetization (susceptibility) measurements.

The Fe^{2+} ion has six electrons in 3d-orbitals outside closed electronic shells. Since the five 3d-orbitals can accept ten electrons, there are 10!/(6!4!) ways of accommodating six electrons; this results in 210 distinct states. To treat all of them would pose a formidable theoretical problem. We have made, therefore, the commonly accepted assumption that the ground state is a 2S + 1, i.e., fivefold (quintet) state that is energetically far removed from the next higher quintet state. With this assumption the spin Hamiltonian formalism (Abragam and Bleaney, 1970) provides a good description of the ground state manifold. Whether this description is applicable to our case has been examined in detail in Appendix A. The spin Hamiltonian predicts the energy levels and magnetization of the quintet state in terms of axial (D) and rhombic (E) crystalline field parameters and an electronic g-value that reflects the influence of an external magnetic field on the states.

In reduced RCs, the primary quinone contains an additional electron that interacts magnetically with the moment of the Fe^{2+}. We have assumed an exchange interaction, J, between the two spin systems. Depending on the sign of this interaction, one expects either an increase or decrease of the magnetization compared to the value predicted from an uncoupled system.

The magnetization of RCs with varying amounts of quinones, both in the unreduced and reduced state, was measured in the temperature range between 0.7° and 200°K and magnetic fields up to ~10 kG. The data were analyzed in terms of the crystalline field parameters D, E,

electronic g-value, and exchange interaction, J. From the values of these parameters, the symmetry of the iron site and the interaction of the Fe and the quinones was inferred. A preliminary account of this work has been presented earlier (Butler et al., 1978).

MATERIALS AND METHODS

Sample Preparation

Reaction centers were prepared from *Rhodopseudomonas sphaeroides* R-26 by extraction with the detergent, LDAO, as previously described (Feher and Okamura, 1978). Samples containing ~0, 1, and 2 quinones per RC were prepared according to the procedure of Okamura et al. (1975). The optical absorbances of the RCs after final DEAE cellulose purification were typically $A_{802}^{1\,cm} = 100$; further concentrations to $\sim A_{802}^{1\,cm} = 250$ was accomplished by either vacuum dialysis at 4°C using 25,000 mol wt cutoff collodian bags (Schleicher and Schuell, Keene, N.H.) or by ultrafiltration using an Amicon M-3 cell with PM10 membranes (Amicon Corp., Lexington, Mass.). In several samples the detergent LDAO was exchanged with Triton X-100 by adsorption to DEAE cellulose equilibrated with 10 mM Tris-Cl, pH 8, 0.1% Triton X-100 (TT buffer), followed by elution with 1 M NaCl, TT buffer and dialysis to remove the salt. For the Triton exchanged samples, up to 75% of the free Triton was retained during concentration; consequently, the Triton concentration increased during concentration, although it remained <1%. The concentrated samples were weighed into a delrin bucket of the magnetometer. All samples were deoxygenated by freezing in liquid nitrogen, exchanging the atmosphere above the sample with argon, thawing, stirring, and refreezing. This procedure was repeated at least twice. Samples were kept at 77°K until ready to run.

Reduced RCs were prepared with sodium dithionite. Since LDAO reacts with dithionite, it was exchanged with Triton X-100, as described above. The reduction was accomplished by adding under anaerobic conditoins 20 μl 1 M sodium dithionite in 1 M Tris-Cl, pH 8, to a preweighed sample of RCs. After stirring for a few seconds, the sample was frozen in liquid nitrogen. The extent of reduction was determined by EPR (see Results).

Quinone Analysis

Three different methods were used to determine the content of quinone in RCs:

PHOTOOXIDATION OF CYTOCHROME *C* Reduced cytochrome is photooxidized when RCs are illuminated (Parson, 1968). The number of cyts oxidized per RC depends on the number of electrons transferred, i.e., on the number of quinones. Since Q_1 can accept one and Q_2 two electrons (e.g., Parson, 1978), one obtains the following relation which was experimentally verified:

$$\text{For } Q < 1.0 \qquad Q/\text{RC} = \text{cyt oxidized/RC}$$

$$\text{For } 1.0 < Q < 2.0 \qquad Q/\text{RC} = (\tfrac{1}{2})(\text{cyt oxidized/RC} + 1).$$

Ten μl of reduced horse heart cyt c (1 mM, Sigma Type 3; Sigma Chemical Co., St. Louis, Mo.) was added to 1 ml of RCs (5 μM) and cross-illuminated with red light (Corning CS-2-64 filters and 500-W tungsten lamp; Corning Glass Works, Science Products Div., Corning, N.Y.) in a kinetic spectrophotometer (McElroy et al., 1974) or Cary 14R. From the rapid change in the absorbance at 550 nm, the number of cyt cs oxidized per RC was obtained from the relation:

$$\text{cyt } c \text{ oxidized/RC} = (\Delta A_{550}/A_{802}^{RC})(\epsilon_{800}^{RC}/\epsilon_{550}^{(ox\text{-}red)cyt}) = 14.4(\Delta A_{550}/A_{802}).$$

KINETICS OF CHARGE RECOMBINATION The kinetics of recovery of the oxidized primary donor after a fast laser pulse proceeds with a characteristic time of ~100 ms when the electron comes from Q_1 and ~1.5 s when it comes from Q_2. Thus, by deconvoluting the biphasic kinetics of recovery, the number of quinones was determined (Blankenship and Parson, 1979). RCs were illuminated at 620 nm

by single turnover laser flashes (Phase *R*, DL 2100C) and the absorbance change at 865 nm was recorded with a kinetic spectrophotometer (McElroy et al., 1974).

CHEMICAL ANALYSIS Quinone was extracted according to Takamiya and Takamiya (1969) and the amount was determined optically (Pumphrey and Redfearn, 1960).

The accuracy of methods *a* and *b* is ±3% or 0.03 quinones, whichever is larger; the accuracy of method *c* is ~3 times less. The *Q*-content of samples UT2 and RT2 was determined by method *c*, the rest by methods *a* and *b*.

Metal Analysis

After the magnetic measurements were completed, the entire samples were thawed and diluted volumetrically in their respective buffers to $\sim A_{802}^{1\,cm} = 10$. To completely solubilize the reduced samples, 0.2% SDS, 1 mM EDTA was added to the TT buffer. As a check, the total sample that was removed was also weighed. The Fe and Mn concentrations of a calibrated aliquot of the diluted sample were determined by atomic absorption spectroscopy (Varian Techtron, Model AA-5, Varian Associates, Instrument Div., Palo Alto, Calif.). Standard solutions used from various sources (Alfa-Ventron, Danvers, Mass.; Fisher Scientific Co., Pittsburgh, Pa.; Arro Labs, Inc. Joliet, Ill.) agreed to within ±2%. The estimated error of the Fe and Mn determinations was ±2% and ±5%, respectively.

The amount of heme iron in the samples was determined by a modified pyridine hemochromagen assay (Bartsch, 1971); the NaOH-pyridine mixture was deoxygenated and reduced with ascorbate instead of Na-dithionite. All samples were found to contain <0.03 heme/RC, which was the sensitivity limit of the method.

The Magnetometer

A Faraday magnetometer of local design was used (Wohlleben and Maple, 1971). The force F_s on a paramagnetic sample in a field with a gradient dH/dz normal to the field is given by

$$F_s = M(dH/dz), \tag{1}$$

where M is the magnetic moment of the sample. The field gradient was produced by Henry-type pole pieces attached to an electromagnet capable of producing a field of up to ~10 kG. The temperature of the sample space could be controlled between 300° and 0.7°K; temperatures below 1.3°K were obtained by pumping on ^{3}He.

The RC sample was contained in a delrin bucket suspended from the balance by a 1-mm diam quartz fiber connected to a 0.5-m diam stainless steel tube. The sample space was precooled to 100°K; the sample which had been kept at 77°K was then transferred and the sample space was evacuated and refilled with ^{3}He to a pressure of 150 mTorr. The force on the sample was transmitted to a microbalance whose pan weights could be varied in 1-mg increments. The force was measured by recording (in addition to the pan weights) the deflection of the microbalance which was translated into a voltage via an inductive pickup transducer. The voltage was calibrated with 1-mg pan weights. The sensitivity of the force measurements was 0.002 mg with a precision of ±0.01 mg. The absolute accuracy, including drifts over long times and larger changes in force, was ±0.02 mg.

The product $H(dH/dz)$ was determined for different magnet currents with an accuracy of ±1% by using standard samples of Al, Ta, Pd, and Pt (~99.999% purity). The field gradient (dH/dz) was calibrated vs. magnet current with an accuracy of ±2% using a standard Ni sphere (99.999% purity) having a magnetization of 20°C of 54.39 G cm^3/g (Bleil, 1963). From these two measurements the magnetic field, H, was obtained with an accuracy of ~±2%.

The temperature of the copper-clad sample chamber was monitored with three thermometers located near the sample. For 30°K < T < 300°K a Pt, for 1.4°K < T < 30°K a Ge, and for 0.7°K < T < 1.4°K a carbon thermometer was used. The accuracy of the temperature determination was ±0.05°K for T > 2.5°K and ±2% for T < 2.5°K. A check of possible temperature gradients between the sample and the thermometers was made in the temperature region between 4°K < T < 25°K by suspending a separate Ge thermometer in the bucket and comparing its reading with the Ge thermometer of the instrument. The measured temperature differences were <0.2%.

THEORY

Energy Levels

Fe^{2+} has six electrons in the five *d*-orbitals leading to a total of 210 states. Application of Hund's rule (maximum occupancy) separates the $L = 2$, $S = 2$ manifold to form a set of $(2L + 1)(2S + 1) = 25$ lowest lying states. These are grouped into five quintet states that are separated from each other by the interaction of the orbital wavefunction with the crystal field. If the lowest lying quintet state is sufficiently separated in energy from the other states, the ground state can be described by an effective spin Hamiltonian (Pryce, 1950; Abragam and Bleaney, 1970). We have used this simplification in our analysis; the justification of it is discussed in Appendix A.

THE UNREDUCED ACCEPTOR Q-Fe^{2+} The spin Hamiltonian for this case is given by

$$\mathcal{H}_u = D_u[S_z^2 - \tfrac{1}{3}S(S+1)] + E_u(S_x^2 - S_y^2) + g_u\mu_B\overline{H}\cdot\overline{S}, \qquad (2)$$

where H is the externally applied magnetic field, μ_B is the Bohr magneton, g_u is the electronic *g*-value of Fe^{2+} which is assumed to be isotropic, $S = 2$ for high-spin Fe^{2+}, and D_u and E_u are the axial and rhombic crystal field parameters. The molecular coordinate system is specified by the crystal field terms, i.e., the magnetic field is expressed in components along the directions established by the spin operators S_x, S_y, and S_z.

The energy levels in the absence of an external magnetic field are given by the eigenvalues E_i, $i = 1, 2 \ldots 5$ of the matrix representation $\mathcal{H}_u$, with $H = 0$, among the basis states $|S, m_s\rangle, m_s = -2, -1 \ldots +2$. These are shown in Fig. 1 for different values of E/D, for $D > 0$ and $D < 0$. The range of physically distinct values of E/D is restricted to $0 \leq E/D \leq 1/3$

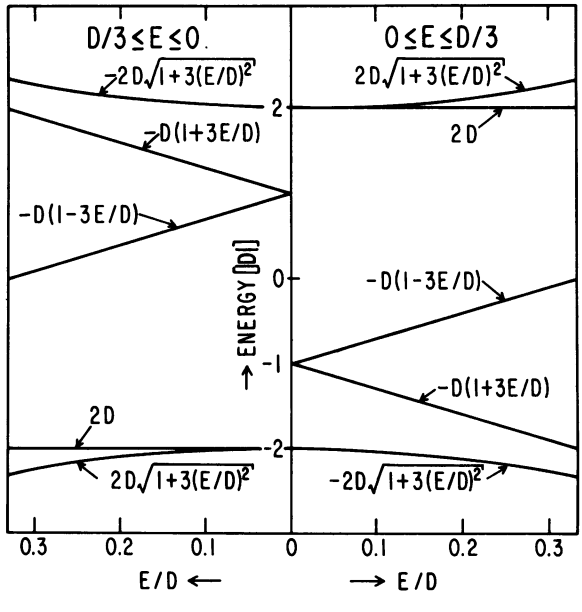

FIGURE 1 Energy levels of the lowest quintet state of high-spin Fe^{2+} vs. E/D in the absence of an external magnetic field for $D > 0$ (right) and $D < 0$ (left). Energies (in units of D) were calculated from the spin Hamiltonian given by Eq. 2.

(Brill, 1977). Any value that is larger than this can be reduced to fall within that interval by a rotation of the axes. At $E/D = 0$, the energy levels invert when the sign of D is changed. At $E/D = 1/3$, the energy levels are the same for positive and negative Ds. For this case, it is therefore meaningless to talk about the sign of D.

The energy levels in the presence of an external field depend on the direction of H with respect to the axis of quantization imposed by the crystal field. The results are shown in Fig. 2 for the three principal directions, assuming particular values for D and E/D (the actual values determined from experiment).

THE REDUCED ACCEPTOR Q^--Fe^{2+} When RCs are reduced, the moment of the electron on the ubisemiquinone Q^-, ($S_1 = 1/2$) must be considered in addition to the Fe^{2+} ($S = 2$). This requires the addition of two terms to the spin Hamiltonian. One is the Zeeman term of the unpaired electron and the other represents the magnetic interaction between the two moments. Assuming an isotropic exchange interaction, $-J\bar{S} \cdot \bar{S}_1$, the spin Hamiltonian for the reduced RC is given by:

$$\mathcal{H}_r = D_r[S_z^2 - \tfrac{1}{3}S(S+1)] + E_r[S_x^2 - S_y^2] + g_r\mu_B\bar{H} \cdot \bar{S} + g_1\mu_B\bar{H} \cdot \bar{S}_1 - J\bar{S} \cdot \bar{S}_1, \quad (3)$$

where the coupling constant J is positive for ferromagnetic coupling. The ground state manifold now comprises ten energy levels given by the eigenvalues of the matrix representation of $\mathcal{H}_r$ among the product states $|S, m_s, S_1, m_{s_1}\rangle$ (Corio, 1966).

The energy levels for a given (relevant to our case) set of values of D, E/D, and J are shown in Fig. 3. Since the system has now an odd number of electrons, the ground state is a Kramers doublet, the two energy levels corresponding approximately to the spin up and spin down states of the unpaired electron on the quinone. Microwave transitions between these two levels produce the observed broad EPR $g = 1.82$ signal (see arrows in Fig. 3) (Okamura et al., 1975 and 1978). The large spectral width arises from the anisotropy of the interaction of the Fe^{2+} with the external magnetic field.

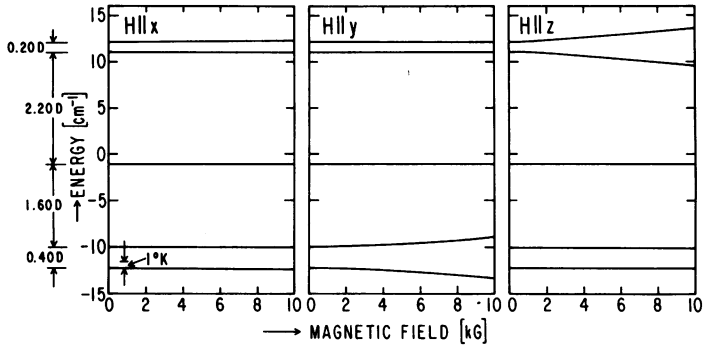

FIGURE 2 Energy levels (obtained from Eq. 2) of the lowest quintet state of high spin Fe^{2+} vs. magnetic field for the three principal axes. The crystal field parameters of the unreduced RC sample UT1 were used in the calculations ($D = 5.52$ cm^{-1}, E = 1.47 cm^{-1}, $g = 2.17$). The magnetization due to level i is obtained from the slope $\partial E_i/\partial H_i$ (Eq. 4). The energy corresponding to a temperature of 1°K is shown in the left panel. At the lowest temperatures of our experiments (0.67°K) essentially only the lowest level is occupied.

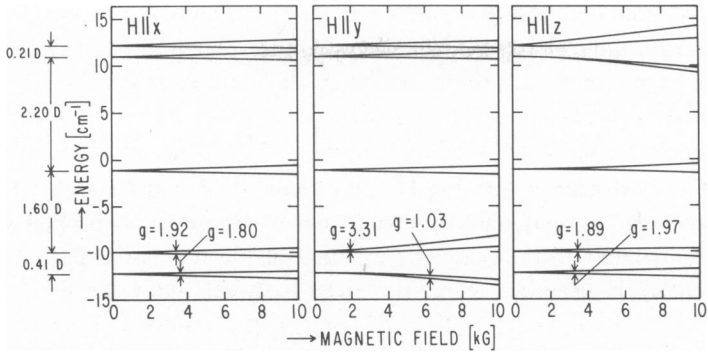

FIGURE 3 Energy levels of the coupled system Q_1^- ($S = ½$) and Fe^{2+} ($S = 2$) described by Eq. 3. The parameters of the reduced RC sample RT1 were used in the calculations ($D = 5.52\ cm^{-1}$, $E = 1.47\ cm^{-1}$, $g = 2.17$, $J = -0.2\ cm^{-1}$). The position at which EPR transitions are expected to occur at 9.0 GHz are indicated by arrows.

The Magnetization

The magnetization can be obtained from the energy levels by the general expression (e.g., Van Vleck, 1932):

$$\mu_i = -\frac{\partial E_i}{\partial H}, \tag{4}$$

where μ_i is the magnetic moment contributed by state i, having an energy E_i. To calculate the magnetization of the quintet state we have to sum up the contributions of all five states, taking into account their respective populations given by the Boltzmann factor, i.e.,

$$\mu(\theta, \phi) = \frac{\sum_{i=1}^{5} -\frac{\partial E_i(\theta, \phi)}{\partial H} e^{-E_i(\theta,\phi)/(k_B T)}}{\sum_{i=1}^{5} e^{-E_i(\theta,\phi)/(k_B T)}}, \tag{5}$$

where k_B is Boltzmann's constant and θ and ϕ are the polar and azimuthal angles of $\overline{H}$ with respect to the crystal field axes. Since the RCs are randomly oriented, we have to average over the direction of the magnetic field. Thus, the total magnetic moment is given by

$$M = N\mu_{ave} = N\frac{2}{\pi}\int_0^{\pi/2}\int_0^{\pi/2} \mu(\theta, \phi) \sin\theta \, d\theta \, d\phi, \tag{6}$$

where symmetry requirements reduced the integral from the entire sphere to one octant (Lefebvre and Maruani, 1965). The evaluation of Eqs. 5 and 6 is carried out by numerical techniques as described in Appendix B. When the temperature is larger than the energy splittings of the ground state quintet, the crystal field splittings can be neglected, the spin system can be viewed as essentially degenerate and the problem simplifies considerably. It is, therefore, convenient to treat the high temperature and low temperature results separately, as we show below.

High temperature magnetization. The temperature region over which this treatment is valid is given by

$$\mu_B H, \Delta E_q \ll k_B T \ll \Delta E_x, \tag{7}$$

where ΔE_q is the total energy splitting of the ground state quintet and ΔE_x is the energy difference between the ground state quintet and the first excited multiplet state. The only paramagnetic contributor to the magnetic moment of the RC is the Fe^{2+} ion. Its effective magnetic moment μ_{eff} is given by, e.g., Carlin and van Duyneveldt (1977):

$$\mu_{\text{eff}} = \mu_B g_u \sqrt{S(S+1)}, \tag{8}$$

where again for simplicity g_u has been assumed to be isotropic, although in reality it has three components, g_x, g_y, and g_z (see Appendix A) which are related to the measured average value by

$$g_u^2 = \tfrac{1}{3}(g_x^2 + g_y^2 + g_z^2). \tag{9}$$

In this temperature regime, $k_B T \gg \mu_{\text{eff}} H$, hence the magnetic moment, M, is given by Curie's law:

$$M = N\mu_{\text{eff}}^2 H/(3k_B T), \tag{10}$$

where N is the number of Fe^{2+}. The force on this magnetic moment, F_s, is given by

$$F_s = M\frac{dH}{dz} = N\mu_{\text{eff}}^2\left(H\frac{dH}{dz}\right)\Big/(3k_B T). \tag{11}$$

Thus, by plotting F_s vs. $1/T$, one obtains from the slope the value of μ_{eff}^2 and hence g_u.

Low temperature magnetization. When the thermal energies become comparable to or smaller than the crystal field splittings, i.e., when

$$k_B T \leq \Delta E_q, \tag{12}$$

the energy levels of the quintet state have to be considered in detail, i.e., Eqs. 5 and 6 have to be used to evaluate the magnetization. Note that for the unreduced acceptor all energy levels approach the origin ($H = 0$) with zero slope (see Fig. 2), i.e., Fe^{2+} does not have a magnetic moment near zero field (see Eq. 4). Thus, one can picture the external magnetic field as inducing a magnetic moment in the Fe^{2+} of the RCs. This is in contrast to an ion having an odd number of electrons whose ground state Kramer's doublet is degenerate at $H = 0$. We also see from Fig. 2 that at low temperatures the biggest contribution to the magnetization comes from those RCs whose y-axes point along H. This is a consequence of the large value of E/D. We can see this qualitatively by rewriting the spin Hamiltonian Eq. 2 for $E/D = 1/3$ in the absence of an external magnetic field as $\mathcal{H}_u = -(2/3)\, D\, S_y^2 + (2/3)\, D\, S_z^2$. Classically, this Hamiltonian gives the lowest energy for the Fe^{2+} spin aligned equally likely along the $+y$ and $-y$ directions. The application of a field along the y-axis easily rotates spins from one direction to the other, thereby giving rise to a large magnetization. On the other hand, application of a field normal to the y-direction produces only a slight realignment of the spins.

As the temperature is lowered, the populations of the excited states drop and μ, the magnetic moment per Fe^{2+} at constant H, reaches a limiting (saturation) value at a temperature at which only the lowest state of the quintet is populated. Thus, a detailed fit of the magnetization vs. temperature provides information about the energy levels from which the parameters D_u and E_u of the spin Hamiltonian can be determined.

Instead of performing a detailed fit of μ vs. T (as has been done in this work), one can estimate the range of D and E from the low temperature saturation magnetization. Fig. 4 shows the theoretical magnetic moment Eqs. 2, 4, and 6 of the lowest level (i.e., the saturation moment) vs. D for different values of E/D. At $D = 0$, $\mu = g\, m_s = 4.34$ Bohr magnetons. As D increases, μ decreases. The reason is that the slope $\partial E_i/\partial H$ of the lowest state and hence its magnetic moment (Eq. 4) arises from an admixture of the next higher state by the magnetic field. The larger D, the larger the energy splitting to the higher state and hence the smaller the admixture. For $D < 0$ and $E/D = 0$, the magnetic moment reaches a constant value since for this case the lowest state is doubly degenerate ($m_s \pm 2$).

THE REDUCED ACCEPTOR Q^--Fe^{2+}

High temperature magnetization. In the high temperature limit we require for the reduced acceptor in addition to the condition given by Eq. 7 that the magnetic interaction between the unpaired electron on Q and Fe^{2+} be smaller than k_BT. If we assume this to be an exchange interaction of strength J, then

$$|J|\bar{S} \cdot \bar{S}_1 \ll k_BT. \tag{13}$$

In our case, $|J|S \cdot S_1 \ll \Delta E_q$; Eq. 13 is satisfied whenever Eq. 7 holds. Since we neglect in this

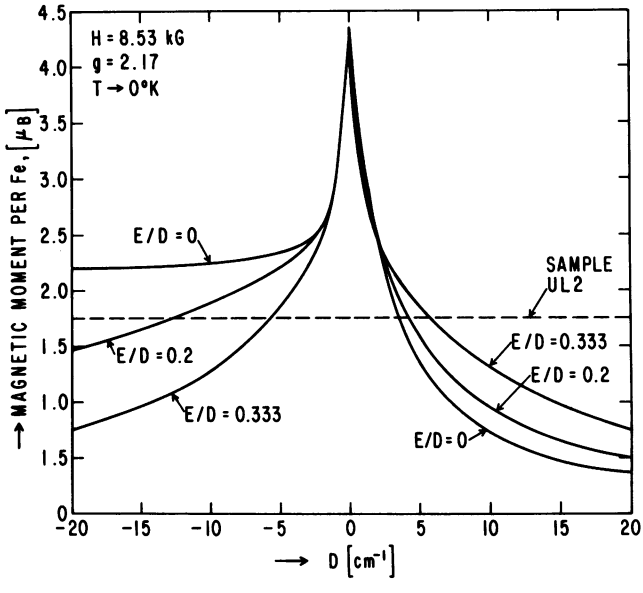

FIGURE 4 The calculated (Eqs. 2, 4, and 6) magnetic moment per Fe (in Bohr magnetons) of the lowest level of high spin Fe^{2+} at 8.53 kG and $g = 2.17$ vs. different values of D and E/D. The graph enables one to estimate from the low-temperature magnetization the acceptable regions of D and E. The broken line represents the observed μ for the unreduced RC sample UL2.

temperature regime the magnetic interaction between the two spins, the effective magnetic moment squared that appears in Eq. 11 is given by the sum of the individual contributions:

$$\mu_{\text{eff}}^2 = \mu_B^2[g_r^2 S(S+1) + g_1^2 S_1(S_1+1)] = \mu_B^2[6\, g_r^2 + 0.75\, g_1^2], \tag{14}$$

where g_r and g_1 are the g-values of the Fe^{2+} and Q^-, respectively. The force is obtained by substituting Eq. 14 into Eq. 11. Since g_1 is known to have a value of 2.0049 (Feher et al., 1972), the only unknown quantity to be determined from experiment is g_r.

Low temperature magnetization. The spin Hamiltonian for this case is given by Eq. 3 and the energy levels are shown in Fig. 3. Since the ground state splittings of the Kramers doublet is relatively small, the magnetization does not saturate even at the highest magnetic fields (H = 8.53 kG) and lowest temperatures (T = 0.67°K) used in these experiments. From a fit of the experimental data with theory the parameters D_r, E_r, and J can be determined. The difficulties associated with this three-parameter fit are discussed in the next section.

EXPERIMENTAL RESULTS

Sample Composition

Magnetization measurements were performed on eight RC samples that varied in their quinone content, detergent, and oxidation state. Their relevant chemical and physical properties are summarized in Table I. The cytochrome concentration of all samples was <3% and its contribution to the magnetization was neglected.

The extent of reduction of the primary quinone was determined by measuring the amplitude of the light-induced EPR signal of the donor and comparing it to the signal

TABLE I
CHEMICAL AND PHYSICAL PROPERTIES OF RC SAMPLES

Sample	Oxidation state*	Detergent	UQ/RC‡ ± 3%	$A_{802}^{1\,cm}$ ± 1%	Weight of sample ± 0.1%	Total No. Fe × 10^{-17} ± 2%	Fe/RC§ ± 3%	Total No. Mn × 10^{-17} ± 5%	Mn/RC§ ± 5%
					(g)				
UL0	u	LDAO‖	0.10	222	0.342	1.54	0.97	0.060	0.04
UL1	u	LDAO‖	1.10	269	0.371	1.91	0.92	0.078	0.04
UL2	u	LDAO‖	1.81	252	0.375	1.79	0.91	0.074	0.04
UT1	u	Triton¶	1.02	263	0.374	1.88	0.91	0.041	0.02
RT1	r	Triton¶	1.02	253	0.327	1.61	0.93	0.036	0.02
UT2	u	Triton¶	1.6	243	0.375	1.75	0.92	0.035	0.02
RT2	r	Triton¶	1.6	243	0.370	1.73	0.92	0.035	0.02
ULØ1	u	LDAO + o-phen.‖	0.93	228	0.356	1.62	0.94	0.050	0.03

Quoted errors represent one standard deviation of the mean.
*u = unreduced, r = reduced with Na-dithionite.
‡±3% or ±0.03 UQ/RC, whichever is larger. For samples UT2 and RT2 the errors are ±10% (from chemical determination after concentration and dilution.)
§Based on an extinction coefficient ϵ_{802} = 288 $mM^{-1}\,cm^{-1}$ (Straley et al., 1973).
‖LDAO is 0.025% LDAO, LDAO + o-phen. is 0.025% LDAO + 10 mM ortho-phenanthroline.
¶TRITON is 0.1% TRITON X-100 before concentration of sample.

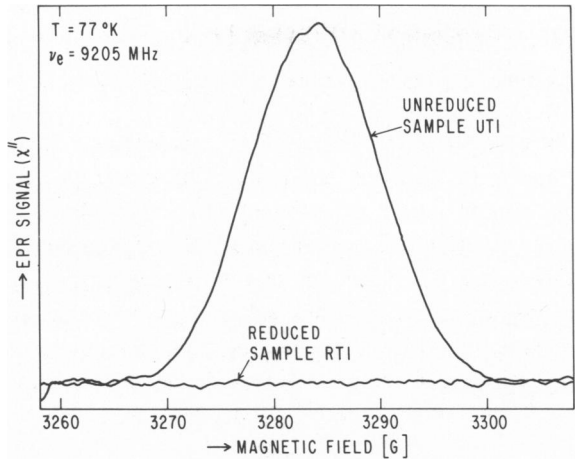

FIGURE 5 The light induced $g = 2.0026$ EPR signal for the unreduced sample UT1 and reduced sample RT1. From the amplitudes of the two signals and the signal-to-noise ratio the extent of reduction was estimated to be at least 98%. To eliminate cavity and other backgrounds, light (instead of magnetic field) modulation was used (McElroy et al., 1970; Feher, 1971).

obtained before reduction. Fig. 5 shows the results after a typical reduction. From the absence of the EPR signal in the reduced sample and the observed signal-to-noise ratio, the degree of reduction (>98%, in this case) was determined.

Data Reduction

The results of a typical measurement of the force F vs. temperature at constant H and dH/dz are shown in Fig. 6. There are three contributions to F:

$$F = F_S + F_{IMP} + F_0, \tag{15}$$

where F_S is the force of interest due to the paramagnetism of RCs, F_{IMP} is the temperature

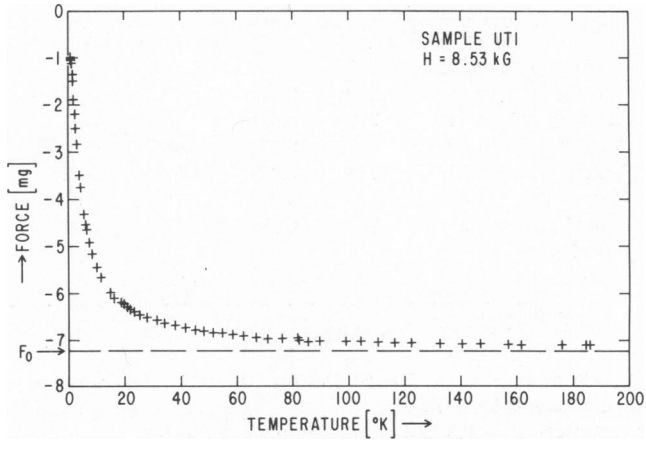

FIGURE 6 Magnetometer force vs. temperature at $H = 8.53$ kG for a typical RC sample (UT1). The temperature independent force, F_0, is shown by the broken line.

dependent force due to paramagnetic impurities, and F_ϕ is a temperature independent force due to the diamagnetism of the sample and sample holder plus a possible temperature independent Van Vleck paramagnetism (Van Vleck, 1932).

The value of F_0 was obtained from the intercept of a plot of magnetization vs. inverse temperature (see Fig. 7 and next section). The error in F_0 was determined from a least square fit of this plot by assigning to each force measurement an uncertainty of ±0.02 mg (see discussion of magnetometer).

The value of F_{IMP} was determined experimentally by measuring the magnetization of buffer solutions containing no RCs. F_{IMP} was found to be the same with or without Na-dithionite added to the buffer. For the full temperature range 200°K > T > 0.7°K, F_{IMP} amounted to no more than 4% of F_S. At H = 8,530 G, the field at which most of the experiments were performed, F_{IMP} was described by

$$F_{IMP} = \begin{cases} \dfrac{0.7}{T} \text{ mg} \pm 25\% & T > 1.9°\text{K} \\ 0.37 \text{ mg} \pm 25\% & T < 1.9°\text{K}. \end{cases} \tag{16}$$

To determine the origin of the impurity force, an empty bucket precooled to 77°K in liquid N_2 was transferred in air into the magnetometer at low temperatures. The impurity force was

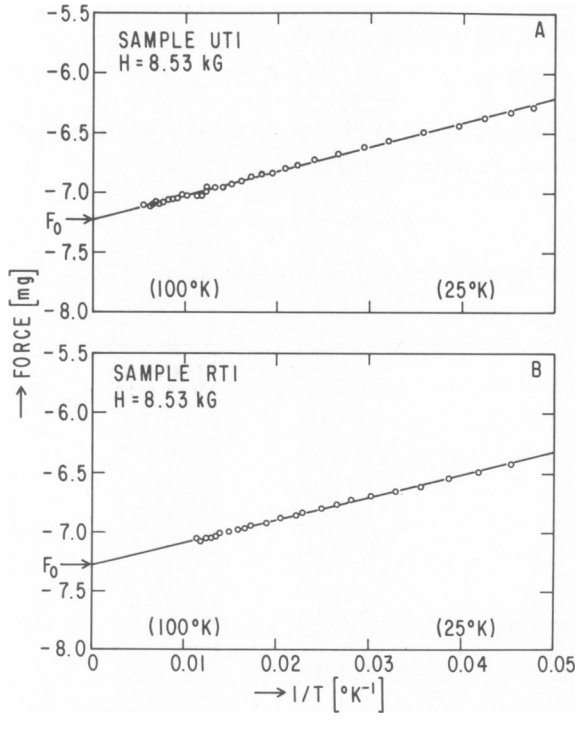

FIGURE 7 Magnetometer force vs. $1/T$ for unreduced (A) and reduced (B) RCs in the high temperature region (T > 20°K). The solid line represents the linear least square fit to Curie's law (Eq. 11) with μ_{eff} as the slope parameter. The temperature independent force, F_0, is obtained from the intercept as shown. Similar analyses were performed on the other samples (see Table II).

found to be the same as obtained with buffer. However, when the empty bucket was transferred at room temperature, F_{IMP} was reduced to zero. The most likely explanation of these observations is that F_{IMP} is mainly due to molecular oxygen that condensed on the sample holder during the low temperature transfer. From the known susceptibility of O_2 (Cooke et al., 1954; Meyer et al., 1957), we estimated that $\sim 10^{16}$ molecules of O_2 could account for F_{IMP}.

The experimental errors were analyzed by assuming statistical independence of the individual contributions, e.g.,

$$\sigma_{F_S}^2 = (\sigma_F^2 + \sigma_{F_{IMP}}^2 + \sigma_{F_0}^2), \tag{17}$$

where σ represents 1 SD.

At low temperatures a useful quantity in interpreting the experimental results is the magnetic moment per Fe, μ. It is determined from the experimental force by (see Eq. 1)

$$\mu = F_s/[N(\mathrm{d}H/\mathrm{d}z)]. \tag{18}$$

The experimental error associated with μ was determined by combining the errors in F_s, N, and $\mathrm{d}H/\mathrm{d}z$, assuming again statistical independence. Specific details of the error analysis are given in the next section and Appendix B.

High Temperature Magnetization—The g-value of Fe^{2+}

The measured force F vs. reciprocal temperature for $T > 20$°K at $H = 8.53$ kG for a typical unreduced RC sample is shown in Fig. 7 *A*. The solid line represents the linear least square fit to the data. The effective magnetic moment, μ_{eff}, of the Fe^{2+} is determined from the slope of the line according to Eq. 11. The error in μ_{eff} was obtained by combining the errors in the force measurements (Eq. 17) with the uncertainties in N, ($H\,\mathrm{d}H/\mathrm{d}z$), and T.

For reduced samples (e.g., see Fig. 7 *B*), there is an additional contribution to the magnetization from the Q_1^--radical ($S = \frac{1}{2}$) which must be subtracted to obtain the moment for Fe^{2+} (the second quinone Q_2 accepts two electrons (Q_2^-) and is, therefore, not paramagnetic). However, since the force is proportional to the square of the moment, the Fe^{2+} ($S = 2$) dominates the high temperature magnetization (Eq. 14). Furthermore, since the magnetic moment of Fe^{2+} in reduced and unreduced RCs is approximately the same, an error in the degree of reduction produces only a relatively small change in the measured magnetization and, hence, a small error in the determination of g_r. For instance, the magnetization of a 90% reduced sample is only $\sim 1\%$ lower than that of a 100% reduced one.

The effective moments and g-values, derived from Eq. 8, of all samples are given in Table II. A relatively small variation in these parameters was obtained.

Low Temperature Magnetization—The Crystal Field Parameters D and E and Exchange Interaction J

THE UNREDUCED ACCEPTOR At low temperatures the ground state quintet of Fe^{2+} is split, resulting in the saturation of the magnetization with applied field. From an analysis of the saturation behavior the values of D and E can be deduced. We used two different experimental procedures. In one, μ was measured at the lowest attainable temperature (0.67°K) as a function of magnetic field and, in the other, μ was determined at a magnetic

TABLE II
MAGNETIC AND CRYSTAL FIELD PARAMETERS OF RCS

Sample	Effective moment of Fe, μ_{eff}* ± 2%	G-value of Fe ± 2%	Saturation moment*‡ per Fe ± 3%	Axial parameter§ D cm^{-1}	Rhombic parameter§ E cm^{-1}	Phombic/axial ratio§ E/D
UL0	5.51	2.25	2.06	3.68	0.97	0.26
UL1	5.24	2.14	1.68	4.85	1.23	0.25
UL2	5.31	2.17	1.75	4.85	1.30	0.27
UT1	5.31	2.17	1.62	5.52	1.47	0.27
RT1	5.29‖	2.16‖	2.16¶	5.28	1.33	0.25
UT2	5.49	2.24	1.78	5.77	1.68	0.29
RT2	5.31‖	2.17‖	2.16¶	5.28	1.33	0.25
ULØ1	5.21	2.13	1.94	3.25	0.69	0.21

For the chemical and physical properties of the sample, see Table I. Quoted errors represent 1 SEM.
*Moment in Bohr magnetons.
‡Measured at 0.67°K and 8.53 kGauss.
§For errors of the fitted crystal field parameters, see Figs. 9 and 11.
‖After subtracting the contribution of the electron spin on Q_1 (see Eq. 14).
¶Reduced samples do not saturate at 0.67°K because of the electron on the ubiquinone.

field of 8.53 kG as a function of temperature. Both procedures gave the same value of D and E. However, the results obtained from the T-dependence were more accurate and will, therefore, be presented.

The experimental results for RCs with ~0, 1, and 2 quinones are shown in Fig. 8. From the experimentally observed saturation moment of 1.7–2.2 Bohr magnetons per Fe^{2+}, an acceptable range of D values can be obtained from Fig. 4. More precise values of D and E were

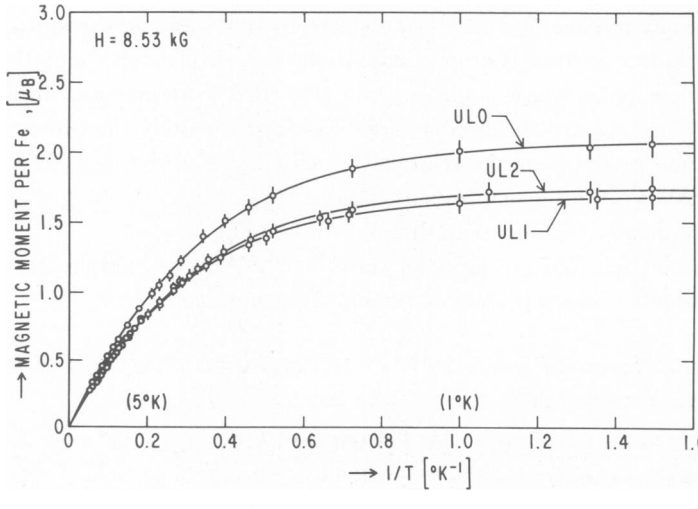

FIGURE 8 Magnetic moment per Fe (in Bohr magnetons) vs. $1/T$ for unreduced RCs having approximately 0, 1, and 2 quinones. Solid lines represent least square fits with D and E as free parameters. The values of D and E for these and other samples are summarized in Fig. 9 and Table II.

obtained by fitting the experimental results with the theoretically calculated magnetic moment (Eqs. 2, 5, and 6). The fit (see solid line in Fig. 8) was obtained with a least squares program (see Appendix B) in which D and E were treated as free variables with the values of g taken from the high temperature data. The values of D and E that gave the best fits are shown in the D-E plane in Fig. 9. The error bars represent the major and minor axes of elipses that encompass a 68% confidence region (see Appendix B for details). Similar results were obtained by treating all three parameters, D, E, and g as free, i.e., by performing a least squares fit in three-dimensional parameter space (Appendix B and Butler, 1980).

The results of Fig. 9 show that the values of D and E are the same for RCs with 1 and 2 quinones. However, removal of Q_1 produced a significant change. The largest change was observed when orthophenanthroline was added to RCs. A relatively small change in D and E was observed when the detergent LDAO was replaced by Triton X-100.

THE REDUCED ACCEPTOR The magnetic moments vs. temperature for the reduced and unreduced sample RT1 and UT1 are shown in Fig. 10. The lack of saturation at low temperatures due to the spin on the Q_1^- of the reduced sample is clearly discernible. The solid and dotted lines represent the calculated moments obtained from a least square (χ^2) fit. For the unreduced sample, the procedure outlined in the previous section was used; for the reduced sample we assumed that D and E did not change on reduction. The best fit (minimum χ^2) was obtained for $J = -0.2 \pm 0.1$ cm^{-1}. The negative sign shows that the spins on Q^- and Fe^{2+} are antiferromagnetically coupled. A similar treatment of samples RT2 and UT2 gave an exchange interaction of $J = -0.3 \pm 0.1$ cm^{-1}.

The antiferromagnetic coupling can be seen qualitatively by comparing the sum of the moments on Q^- and Fe^{2+} (i.e., no interaction) with the observed moment of the reduced sample. This has been done in Fig. 10 where the dashed line represents the sum of the noninteracting moments. Since the experimental points fall below the dashed curve, an antiferromagnetic coupling is indicated. One can estimate the magnitude by J by equating the reduction of the observed magnetic moment to a reduction in the internal magnetic field caused by the exchange interaction. In our case, $(\mu_R - \mu_u)$ is $\sim$¾ of the value expected for a free, noninteracting spin (see Fig. 10). This means that the exchange interaction produces an

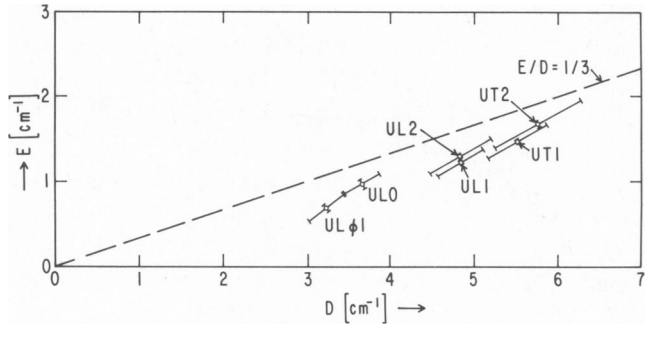

FIGURE 9 Values of the crystal field parameters D and E for unreduced RCs having different detergent, quinone, and orthophenanthroline content. The values were obtained from least square fits to the experimental data as shown in Fig. 8. The error bars represent the major and minor axes of 68% confidence contour ellipses (see Appendix B). The chemical and physical composition of the samples are summarized in Table I and the magnetic parameters in Table II.

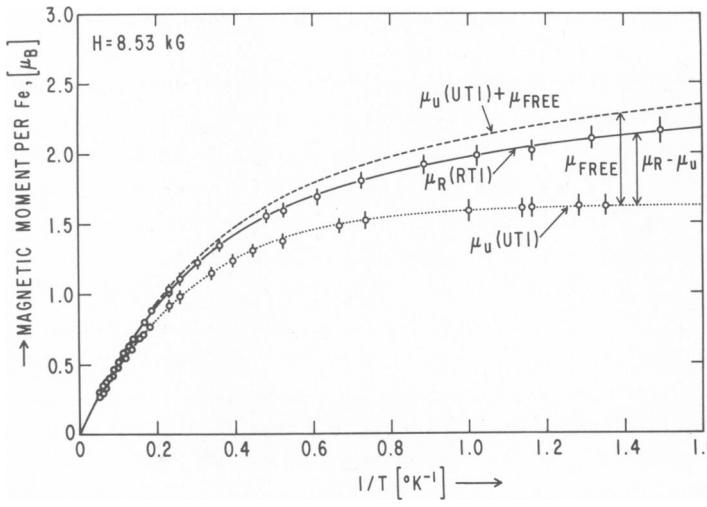

FIGURE 10 Magnetic moment per Fe (in Bohr magnetons) vs. $1/T$ of unreduced (UT1) and reduced (RT1) RCs. Dotted line represents least square fit with D and E as free parameters for the unreduced sample and solid line with J as a free parameter for the reduced sample, assuming that D and E remain unchanged on reduction. The dashed line represents the expected moment for noninteracting spins. The fact that the experimentally observed moment falls below the dashed line implies antiferromagnetic coupling.

effective (and opposite) magnetic field that is ~¼ of the ~8 kG applied field, i.e., ~2 kG. This corresponds to an exchange interaction of ~0.2 cm^{-1}, in agreement with the value obtained from the computer fit.

In the above calculations of J it was assumed that D and E for the reduced and unreduced samples were the same. In principle, we need not make this assumption, but can search for a fit that minimizes χ^2 with D, E, and J as free parameters. Unfortunately, this procedure yielded a value of J with a very large uncertainty (i.e., $\sim\pm 0.4$ cm^{-1}). We, therefore, used a different approach in which we fixed J at different values and calculated the corresponding D and Es. The advantage of this procedure is that if J should become known from a different experiment (e.g., EPR), the values of D and E for the reduced sample could be obtained immediately. The results are shown again with 68% confidence limits in the D-E plane (Fig. 11). The heavy line corresponds to the values of D and E for the unreduced sample. For the range of -0.4 cm$^{-1} < J < 0.2$ cm^{-1} the goodness of fit (i.e., χ^2) does not vary significantly. This again reflects the insensitivity of these measurements to the exact value of J. The basic reason for this insensitivity is the high correlation between D and J, i.e., an increase in D which reduces μ (see Fig. 4) can be compensated by an increase in J and vice versa. Thus, a whole range of values of D and J can generate the same value of μ. However, the experimental data could not be fitted with $|J| > 1$ cm^{-1}.

SUMMARY AND DISCUSSION

To elucidate the electronic structure of Fe in reaction centers, we have measured the static magnetization of both reduced and unreduced RCs from *R. sphaeroides* R-26 over a range of temperatures from 190° to 0.67°K and magnetic fields from 0 to 8.5 kG. Samples were

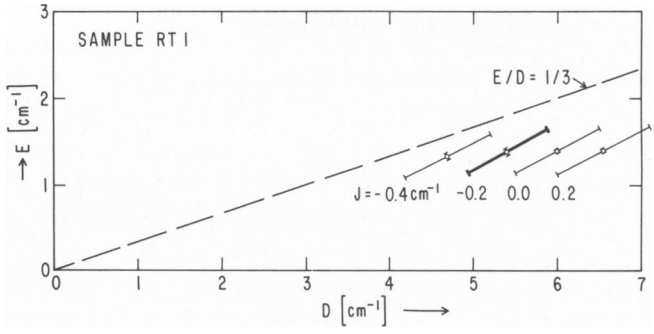

FIGURE 11 Values of D and E for reduced sample RT1 for different strengths of the exchange interaction J. The heavy line ($J = -0.2$) corresponds to the D and E values of the unreduced sample (UT1). Error bars were obtained as discussed in Fig. 9.

prepared with different quinone content in different detergents; one sample was prepared in the presence of orthophenanthroline, which is known to block electron transfer from Q_1 to Q_2 (Parson and Case, 1970). The magnetic parameters determined from the magnetization measurements are summarized in Table II.

The effective magnetic moments, obtained from the high temperature measurements, were in the range of 5.35 ± 0.15 Bohr magnetons for all samples investigated. This value is comparable to those obtained from other high-spin Fe^{2+} complexes (Figis and Lewis, 1960) and hence characterizes the spin ($S = 2$) and valence state ($+2$) of Fe in RCs. Since unreduced and reduced RCs have the same moments, Fe alone cannot be the primary acceptor. This conclusion is in agreement with that obtained earlier from Mossbauer spectroscopy (Debrunner et al., 1975; Feher and Okamura, 1978).

From the low-temperature experiments we determined the crystal field parameters D and E. Their values reflect the environment of the iron and are consistent with the Fe^{2+} residing in an octahedral environment with rhombic distortion, so that none of the principle axes of the crystal field produced by the ligands are equivalent. The large ratio of the rhombic to axial crystal field parameters E/D indicates a high degree of asymmetry.

The same values of D and E were obtained for RCs having one and two quinones. The most likely explanation of this finding is that Q_2 does not ligand directly to iron, although one cannot entirely exclude the possibility that another equivalent ligand replaces Q_2. It seems, however, unlikely that such an exact equivalence would take place.

Differences were found in the values of D and E in RCs having 1 and 0 quinone. There are two possible explanations for this result: (*a*) Fe^{2+} loses a ligand (e.g., Q_1) when Q_1 is removed, and (*b*) a conformation change of the protein takes place when Q_1 is removed. From the magnetization measurements alone one cannot distinguish between these two possibilities; information from other experiments is therefore required. A comparison of EPR results for $Q_1^- - Fe^{2+}$ and $Q_2^- - Fe^{2+}$ shows that the g-values of the signals are the same and the linewidths are similar (although not identical) (Wraight, 1978 *a* and *b*; Okamura et al., 1978). From these results we conclude that the interaction of Fe^{2+} with Q_1 is approximately the same as with Q_2. Since we argued previously that Q_2 does not form a ligand with iron, we infer that Q_1 does not either. The change in D and E when Q_1 is removed seems, therefore, to

be a consequence of distortion at the iron site. It should be noted that the removal of Q_1 requires a much harsher chemical treatment of the RCs than is required to remove Q_2.

When orthophenanthroline was added to RCs having 1 quinone, D and E changed. This, again, could be either due to the bonding of orthophenanthroline to Fe^{2+} or due to a conformational change at the Fe^{2+} site. The latter interpretation is supported by recent measurements of EXAFS which show that there is no change in the number of ligands or average ligand distance when orthophenanthroline is added to Fe^{2+} in RCs (Eisenberger et al., 1980; W. W. Parson and E. Stern, private communication). Thus, assuming that orthophenanthroline and quinone compete for the same binding site, these results are consistent with neither orthophenanthroline nor the secondary quinone binding directly to Fe. It is interesting to note that orthophenanthroline causes a narrowing of the $g = 1.82$ EPR linewidth of $Q_1^- - Fe^{2+}$ (Feher and Okamura, 1978). This could be explained if the linewidth had a contribution from a spread in values of D and E. The lower values of these parameters found in RCs with orthophenanthroline could explain the narrowing of the EPR line.

When the detergent LDAO was replaced by Triton X-100, the values of D and E changed by small but statistically significant amounts (see Fig. 9). Since the bonding of the iron is not expected to depend on detergents, we attribute these results to conformational changes of the RCs.

We have tried to obtain the exchange interaction J between the spins on Q^- and Fe^{2+} from the low-temperature magnetization of reduced RCs. However, the fitting of the experimental results with theory poses some problems of uniqueness since we have three parameters, D, E, and J at our disposal (g is obtained from the high-temperature measurements). Assuming that D and E of the reduced RCs is the same as in the unreduced RCs, we obtained the values of $J = -0.2 \pm 0.1$ cm^{-1} and $J = -0.3 \pm 0.1$ cm^{-1} for RT1 and RT2, respectively. The negative sign indicates antiferromagnetic coupling. In an alternate approach we fixed the values of J and determined the possible values of D and E (see Fig. 11). The quality of a least squares fit did not vary significantly for values of J between -0.4 cm$^{-1} < J < 0.2$ cm^{-1}. This shows that magnetization measurements are not well suited to determine Js that are much smaller than D or E. This indeterminancy can be settled by other experiments, such as EPR spectroscopy, which is more sensitive to the value of J. Preliminary calculations have shown that the $g = 1.8$ value of the broad EPR signal can be obtained by using values of D, E, and J that are similar to the ones obtained in this work (Butler et al., 1978; Butler, 1980).

With the aid of model compounds (Coffman and Buettner, 1979), one can use J to obtain a rough estimate of the distance between Fe and Q^-. For our observed value of $|J| < 1$ cm^{-1}, a distance of >5Å is obtained. This is consistent with the previous conclusion that Q does not bond directly to iron. Recently, Kessel et al. (1980) have measured the exchange interaction between high spin Fe^{3+} and single semiquinone ligands in model complexes. They found a J that is approximately three orders of magnitude larger (-600 cm^{-1}) than that determined in this work for RCs. This, again, points to the conclusion that Q does not bond to Fe^{2+} in RCs.

In all of our low temperature analyses we assumed the validity of the spin Hamiltonian formalism. This approach has been shown to adequately describe the ground state of several high spin Fe^{2+} model compounds (e.g., Champion and Sievers, 1977). However, it was found to be inadequate for the description of deoxy hemoglobin (Huynh et al., 1974; Champion and Sievers, 1980) which reportedly has a low lying (~ 50 cm^{-1}) excited orbital state. To test the

applicability of the spin Hamiltonian to our case, we calculated the 25 energies and eigenstates of the $L = 2, S = 2$ manifold (see Appendix A) which we assumed to be split off in energy from the rest of the states. The lowest five energy levels of the orbital Hamiltonian and the magnetization calculated from them for a particular set of orbital parameters were approximately the same as those obtained from the spin Hamiltonian fitted to the observed magnetization of sample UT1. Using these orbital Hamiltonian parameters, we calculated the position of the first excited quintet state. We found that it lies above the ground state by an energy difference of 340 cm^{-1} (490°K). This is in agreement with the temperature dependence of the quadrupole splitting of the Mossbauer results (Debrunner et al., 1975) which, under simplifying assumptions predicts an energy difference of 460°K. The excited quintet is also sufficiently removed from the ground state quintet to have no observable effect on the magnetization for $T < 200$°K.

In fitting the experimental data with theory, we made the simplifying assumptions that g and J are isotropic. To test the validity of this assumption, we computed the magnetization for a typical sample (UT1), by using both the isotropic g shown in Table II and the nonisotropic g shown in Table IV. The computed values of the magnetization for the two cases differed by less than the error in the experimentally determined value. Similarly, for the reduced sample, RT1, we computed the magnetization for the isotropic J shown in Table II and for an ~50% nonisotropic J (i.e., $J_x = -0.1\ cm^{-1}, J_y = -0.2\ cm^{-1}, J_z = -0.26\ cm^{-1}$). Again, the computed magnetizations differed by less than the error.

TABLE III
PERTURBATION EXPRESSIONS FOR SPIN HAMILTONIAN PARAMETERS IN TERMS OF HAMILTONIAN PARAMETERS

Spin Hamiltonian parameter	Orbital Hamiltonian parameters	
	$\mathcal{D}/3 \le \mathcal{E} \le 0$	$0 \le \mathcal{E} \le \mathcal{D}/3$
D	$-\lambda^2 B_-\left[1 + \left(\frac{A_-}{\Delta}\right)\left(\frac{1}{B_-}\right)\right]$	$-\lambda^2 B_+\left[1 - \left(\frac{A_+}{\Delta}\right)\left(\frac{1}{2B_+}\right)\right]$
E/D	$\alpha\Big/\left[1 + \left(\frac{A_-}{\Delta}\right)\left(\frac{1}{B_-}\right)\right]$	$\alpha\left[1 - \left(\frac{A_+}{\Delta}\right)\left(\frac{1}{2\alpha B_+}\right)\right]\Big/\left[1 - \left(\frac{A_+}{\Delta}\right)\left(\frac{1}{2B_+}\right)\right]$
g_x	$g_e + \frac{2\lambda}{3\mathcal{D}(1+\alpha)}$	$g_e - \frac{2\lambda}{3\mathcal{D}(1+\alpha)}$
g_y	$g_e + \frac{2\lambda}{3\mathcal{D}(1-\alpha)}$	$g_e - \frac{2\lambda A_+}{\Delta}$
g_z	$g_e - \frac{2\lambda A_-}{\Delta}$	$g_e - \frac{\lambda}{3\mathcal{D}\alpha}$

The orbital Hamiltonian parameters and spin Hamiltonian parameters are defined in Eqs. A1 and A3, respectively. The auxiliary quantities used in this table are:

$\alpha = \mathcal{E}/\mathcal{D}, a_\pm^2 = 3\alpha^2/(2 + 6\alpha^2 \pm 2\sqrt{1 + 3\alpha^2})$

$A_+ = a_-^2/\{1 + [\mathcal{D}(1 + 3\alpha + 2\sqrt{1 + 3\alpha^2})/\Delta]\} + a_+^2/\{1 + [\mathcal{D}(1 + 3\alpha - 2\sqrt{1 + 3\alpha^2})/\Delta]\}$

$A_- = 4a_-^2/\{1 - [2\mathcal{D}(1 + \sqrt{1 + 3\alpha^2})/\Delta]\} + 4a_+^2/\{1 - [2\mathcal{D}(1 - \sqrt{1 + 3\alpha^2})/\Delta]\}$

$B_+ = 1/[6\mathcal{D}\alpha(1 + \alpha)]$

$B_- = 1/[3\mathcal{D}(1 - \alpha^2)]$.

TABLE IV

COMPARISON OF SPIN HAMILTONIAN PARAMETERS OBTAINED FROM BEST FIT ORBITAL HAMILTONIAN* WITH THOSE DERIVED FROM THE EXPERIMENTAL μ/Fe USING SPIN HAMILTONIAN

Spin Hamiltonian parameters	From best fit orbital Hamiltonian		From experimental μ/Fe§ using spin Hamiltonian
	Perturbation result‡	Numerical results	
$D\ (cm^{-1})$	4.98	5.72	5.52
E/D	0.297	0.211	0.266
g_x	2.18	2.15‖	—
g_y	2.30	2.26‖	—
g_z	2.04	2.03‖	—
g_{AV}	2.18	2.15	2.17

*Best fit obtained for sample UT1 with orbital parameters. $\Delta = 10{,}000\ cm^{-1}$, $\mathcal{D} = -150\ cm^{-1}$, $\mathcal{E} = -37.5\ cm^{-1}$, $\lambda = -50\ cm^{-1}$ (see Eq. A1).

‡See Table III.

§See Table II.

‖The components of the g-vector were obtained by equating the coefficients of the matrices of the magnetic moment operator $\mu_B(\bar{L} + g_e \bar{S})$ with the matrices of the spin Hamiltonian magnetic moment operator $\mu_B (g_x S_x + g_y S_y + g_z S_z)$.

A further assumption was made in modeling the $Fe^{2+} - Q^-$ interaction with an isotropic exchange (Eq. 3) and neglecting magnetic dipole-dipole interactions. The following argument justifies this assumption: If the magnetic moments of both Fe^{2+} and Q^- were isotropic, a spatial averaging of the dipole interaction over all directions would result in no net contribution to the magnetization. However, since the Fe^{2+} magnetic moment is not isotropic, a contribution to the magnetization can be obtained. Depending on the position of the Q^- with respect to the Fe^{2+} coordinate system established by the crystal field, this contribution can be either positive or negative. An order of magnitude estimate of the distance, r, between Fe^{2+} and Q can be made by equating the 2-kG reduction in magnetic field (see Fig. 10 and accompanying discussion) to the dipolar field $\sim\mu/r^3$. This results in a distance, $r \simeq 1.7$ Å. In view of the evidence that Q is not a ligand of Fe^{2+}, this is an unrealistically small $Fe^{2+} - Q^-$ separation. For a more realistic distance of 5 Å, the dipolar interaction energy would be $\sim 10^{-2}$ cm^{-1}, i.e., only a few percent of the fitted exchange energy.

The total Fe (and Mn) content of the samples was determined with high accuracy. By using the published extinction coefficient of $\epsilon_{802} = 2.88\ mM^{-1}\ cm^{-1}$ (Straley et al., 1973), we found the average content of Fe + Mn/RC to be 0.95 ± 0.01. If all RCs had either an Fe or an Mn substituting for it (Feher et al., 1974), the number should have been 1.00. This discrepancy suggests that the published extinction coefficient is too large by 5%, which is the quoted error in its determination. We suggest, therefore, a modified value for the extinction coefficient of $2.74\ mM^{-1}\ cm^{-1}$. It should be noted that since the total Fe content was measured, the extinction coefficient did not enter into the calculations of the magnetic parameters.

In conclusion, we have obtained from magnetization measurements information concerning the electronic structure of Fe^{2+} in RCs. However, questions concerning the chemical nature of the ligands, their distances, etc., remain unanswered. We know from chemical evidence that the Fe^{2+} is not in a heme nor is it bonded to labile sulfurs as in ferredoxin (Okamura et al.,

1974); Lovenberg, 1973 and 1977). To obtain further information on the structure of the Fe site, other experimental techniques, e.g., x-ray diffraction, EXAFS, and EPR, need to be utilized. Some of these are under investigation. To obtain detailed structural information from the crystal field parameters, D and E, remains a challenge for theorists.

APPENDIX A

Energy Levels and Magnetization of $L = 2$, $S = 2$ Manifold: Comparison with Spin Hamiltonian

We have interpreted the low temperature magnetization of Fe^{2+} in RCs by modeling the ground state with the spin Hamiltonian Eq. 2. This model is strictly valid only when there is a well defined spin quintet ground state. That this is not the case for Fe^{2+} in RCs has been shown from the temperature dependence of the quadrupole splitting in the Mossbauer effect (Debrunner et al., 1975). To understand the implications of these low lying states and to assess the validity of the spin Hamiltonian description, we have investigated the possible electronic states of the Fe^{2+} using a physically reasonable orbital Hamiltonian. The goal of this investigation is to determine if there is a set of orbital states with a quintet ground state with zero field splittings and magnetic field dependence similar to those obtained from a spin Hamiltonian and with excited orbital states that predict the observed temperature dependence of the quadrupole splitting obtained from Mossbauer experiments.

Application of Hund's rules to the 210 possible states of the Fe^{2+} ion separates the $L = 2$, $S = 2$ manifold of 25 states as the ground multiplet of the ion. We model this manifold with the orbital Hamiltonian:

$$\mathcal{H} = \frac{\Delta}{6}(L_x^4 + L_y^4 + L_z^4 - \frac{3}{5} tr\, L_z^4) + \mathcal{D}(L_z^2 - \frac{1}{5} tr\, L_z^2) + \mathcal{E}(L_x^2 - L_y^2) + \lambda \mathbf{L} \cdot \mathbf{S} + \mu_B(\mathbf{L} + g_e \mathbf{S}) \cdot \mathbf{H}, \quad \text{(A1)}$$

where $\mathbf{L}$ is the orbital angular momentum operator and $\mathbf{S}$ is the spin operator. The first term represents the cubic crystal field, the second and third terms the tetragonal and rhombic crystal fields, respectively, the fourth term the spin-orbit interaction and the last term the Zeeman energy. In the limit of

$$|\Delta| \gg |\mathcal{D}|, |\mathcal{E}|, \gg |\lambda| \gg \mu_B H, \quad \text{(A2)}$$

special perturbation techniques were developed by Pryce (1950) that result in a description of the lowest five states of the orbital Hamiltonian by a spin Hamiltonian (compare Eq. 2) of the form:

$$\mathcal{H}_s = D\left[S_z^2 - \frac{1}{3}S(S+1)\right] + E(S_x^2 - S_y^2) + \mu_B (g_x S_x H_x + g_y S_y H_y + g_z S_z H_z), \quad \text{(A3)}$$

where the parameters D, E, g_x, g_y, and g_z are expressible in terms of the orbital Hamiltonian parameters Δ, $\mathcal{D}$, $\mathcal{E}$, and λ of Eq. A1 (see Table III). All attempts to fit the parameters D, E, and g deduced from experiment with those obtained from the perturbation expression (Table III) failed unless λ was of the same order as $\mathcal{D}$ and $\mathcal{E}$. This violated the perturbation condition (Eq. A2) and, forced us to seek other methods to compare the lowest five states of the orbital Hamiltonian with the states of the spin Hamiltonian Eq. 2.

We resorted to computation of exact numerical solutions of the 25 energy levels of the orbital Hamiltonian by the same methods used to compute the spin Hamiltonian energy levels, as described in the text. Fig. 12 shows the energy level splittings for typical values of the parameters Δ, $\mathcal{D}$, $\mathcal{E}$, and λ. Our criteria for agreement between the orbital Hamiltonian ground state and the known spin Hamiltonian ground state for a typical sample (UT1) were fivefold: (*a*) at zero field, the lowest five energy level splittings of the orbital Hamiltonian must closely reproduce the spin Hamiltonian energy level splitting;

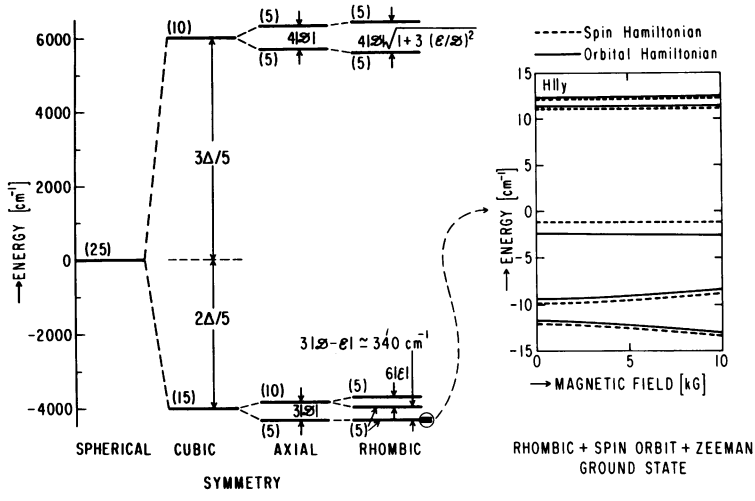

FIGURE 12 Energy level splittings (to scale) of the $L = 2$, $S = 2$ manifold in a crystal field with cubic, axial, and rhombic symmetry. The degeneracy of each level is indicated in parentheses. The best fit with the experimentally observed magnetization of sample UT1 was obtained with the following orbital Hamiltonian parameters: $\Delta = 10{,}000\ cm^{-1}$, $\mathcal{D} = -150\ cm^{-1}$, $\mathcal{E} = -37.5\ cm^{-1}$, $\lambda = -50\ cm^{-1}$. Inset on the right shows energy levels versus magnetic field ($H \parallel y$). Dashed lines were obtained from the spin Hamiltonian.

(*b*) the *g*-value calculated for this orbital ground state must agree with the *g*-value of the spin Hamiltonian. The high temperature effective moment squared $g^2\mu_B^2\, S(S+1)$ is simply the quantum statistical average over the five lowest states of the magnetic moment operator squared, $\mu_B^2\,(L + g_e S)^2$; (*c*) the temperature dependence of the magnetic moment per Fe at constant field must agree within the error bars with the observed values for UT1. This magnetic moment is calculated from the lowest five orbital levels exactly as it is calculated for the spin Hamiltonian description; (*d*) the energy splitting between the orbital ground state quintet and the next higher orbital quintet must explain the observed temperature dependence of the quadrupole splitting measured by Mossbauer spectroscopy (Debrunner et al., 1975); (*e*) the energy splitting between the orbital ground state quintet and the next higher orbital quintet must be sufficiently large to have no effect on the computed magnetization over the temperature range considered, $T < 200°K$.

Taking the value $\Delta = 10{,}000\ cm^{-1}$ for Fe^{2+} (e.g., Orgel, 1966), we systematically searched for values $\mathcal{D}$, $\mathcal{E}$, and λ that produced an orbital Hamiltonian ground state which satisfied the above criteria. We found these criteria to be satisfied for parameters in the vicinity of $\mathcal{D} = -150\ cm^{-1}$, $\mathcal{E} = -37.5\ cm^{-1}$, $\lambda = -50\ cm^{-1}$. To characterize the zero-field orbital ground state quintet, spin Hamiltonian energy splittings were fitted to the orbital splittings using a least squares procedure. This gave the spin Hamiltonian *D* and *E* that best characterize the orbital splittings. Table IV summarizes *D*, *E*, and *g* obtained from the orbital Hamiltonian and compares them with the original parameters deduced by directly fitting the experimental magnetization with a spin Hamiltonian. The agreement is seen to be quite good. The energy levels using these parameters is shown in Fig. 12. The theoretical behavior of the quintet ground state in a magnetic field ($H \parallel y$) is shown in the inset of Fig. 12 (full lines). They are in good agreement with the energy levels obtained from the original spin Hamiltonian (dashed lines). Similar agreement was obtained for *H* in the *x* and *z* directions. Thus, we have satisfied the first two criteria. In accordance with our third criterion the calculated magnetic moment per Fe for the lowest five orbital levels agreed within experimental error with the observed temperature dependence at 8.53 kG, similar to the agreement shown in Fig. 8 for the spin Hamiltonian. (This can also be seen in the agreement of the field dependence, i.e., dE/dH, for the energy levels in the inset of Fig. 12.)

The first excited quintet state was calculated to lie 340 cm^{-1} (490°K) above the ground state (see Fig. 12). A simple model to explain the temperature dependence of the quardupole splitting of the Mossbauer effect predicts a dependence of the form $\tanh(\delta E/2kT) = \tanh(245°/T)$. The observed Mossbauer data could be fitted with $\tanh(230°/T)$ (Debrunner et al., 1975), in good agreement with the calculated energy splitting, satisfying the fourth criterion. Furthermore, levels removed by 490°K would not affect the magnetization for temperatures <200°K, again in accordance with our fifth criterion.

The above results show that the quintet ground state of Fe^{2+} is describable by a spin Hamiltonian that can be derived from a physically reasonable orbital Hamiltonian even though there are relatively low lying excited orbital states. Furthermore, the values of the parameters $\mathcal{D} = -150$ cm^{-1}, $\mathcal{E} = -37.5$ cm^{-1}, and $\lambda = -50$ cm^{-1} are physically reasonable.

APPENDIX B

Numerical Analyses

COMPUTATION OF EIGENSTATES, EIGENVALUES, AND MAGNETIZATION The energy eigenvalues and corresponding eigenstates of the matrix representations of the spin Hamiltonians, Eqs. 2 and 3, were evaluated using path "CH" of the EISPACK package of FORTRAN coded eigenvalue subroutines produced by and available from Argonne National Laboratory (Smith et al., 1976). The derivatives of the energy eigenvalues with respect to field, Eq. 4, were evaluated by the numerical five-point differentiation formulas tabulated by Davis and Polonsky (1964). The powder average integral, Eq. 6, was evaluated on the first octant of the sphere ($0 \le \theta \le \pi/2, \theta \le \phi \le \pi/2$) by two-dimensional Gaussian quadrature (Davis and Polonsky, 1964) over a 16-point net in the θ-ϕ plane; four points in the θ direction and four points in the ϕ direction. The convergence of this integration was checked by using a 64-point net (eight in each direction). The average magnetic moment calculated from the 64 point and 16 point nets agreed to within 0.01%.

LEAST SQUARE FITS IN MULTIDIMENSIONAL PARAMETER SPACE This appendix describes the statistical techniques used to estimate the spin Hamiltonian parameters D, E, and g, that provide the best fit to the measured magnetic moment per RC as a function of temperature T at fixed magnetic field, such as plotted for samples UL1, 2, and 3 in Fig. 8. From the energy levels obtained from the spin Hamiltonian (Eq. 2), the spatially and thermally averaged magnetic moment per Fe^{2+}, $\mu(T; D, E, g)$ is calculated according to Eqs. 5 and 6 (see above). We define the best fit parameters as those which minimize the residual sum of squares:

$$\chi^2 = \sum_{i=1}^{N} [\mu_0(T_i) - \mu(T_i; D, E, g)]^2/\sigma_i^2, \tag{B1}$$

where $\mu_0(T_i)$ is the observed magnetic moment at temperature T_i, N is the total number of experimental points, σ_i is the experimental uncertainty of the observed point, and μ is the theoretical moment which is being fitted, all measured or calculated at the same field strength. The minimization of χ^2 was carried out by a derivative-free analog of the classical Gauss-Newton algorithm for minimization, as described by Jennrich and Ralston (1979) and implemented as program BMDPAR in the BMDP package (Dixon and Brown, 1979). This program computes estimates x_i, ($x_1 = D, x_2 = E, x_3 = g$), of the parameters that give the best fit. We treat all three parameters equally in this derivation but in practice any of them can be fixed, as was done in our analysis with g fixed. Also computed are the correlation matrix ρ_{ij} and the estimated variances S_i^2 of the parameters, which can be combined to give the covariance matrix of the parameters:

$$C_{ij} = s_i s_j \rho_{ij}. \tag{B2}$$

The basic statistical result of this analysis is analogous to the results obtained for a completely linear theory (Jennrich and Ralston, 1979). If δx is the vector (of dimension L) of errors of the estimated parameters from their true values (in this case, $L = 3$, $\delta x = [\delta D, \delta E, \delta g]$), then $(1/L)\delta x^T C^{-1} \delta x$ is a

random variable with the F-distribution $F(L, \text{N-L})$ (Jennrich and Ralston, 1979; Eadie et al., 1971; Bevington, 1969). The P confidence region (centered in the L dimension parameters space at the best fit parameters) is bounded by the surface that is the solution of:

$$\delta x^T C^{-1} \delta x = L \cdot f, \tag{B3}$$

where f is the number such that

$$\text{Prob}\,[\,F(L, \text{N-L}) < f\,] = P, \tag{B4}$$

which can be found from standard statistical tables (Bevington, 1969). To facilitate visualization and plotting of this ellipsoidal confidence region, we diagonalized the matrix C^{-1} so that the various ellipsoidal axes of the confidence region were determined. As described in the text, we also found it useful to project the three-dimensional (D, E, g) ellipsoid to a two-dimensional ellipse in the D-E plane centered at the best fit parameters. The semimajor axes of these ellipses are the plots in Figs. 9 and 11.

The covariance matrix C_{ij} contains all the statistical information for the fitted parameters. In particular, if one wishes to estimate some other quantity expressible in terms of the spin Hamiltonian parameters, both its estimate and standard deviation can be obtained from our analysis. For example, the zero field splitting of the lowest two energy levels of the spin Hamiltonian (see Fig. 1) is given by

$$E_{01} = D[2\sqrt{1 + 3(E/D)^2} - 1 - 3(E/D)]. \tag{B5}$$

An estimate of E_{01} is obtained by substituting the best fit estimates of D and E in Eq. B5. For small changes in the parameters, Eq. B5 can be linearized to give

$$\sigma^2_{E_{01}} = (\partial E_{01}/\partial D)^2 C_{DD} + (\partial E_{01}/\partial E)^2 C_{EE} + 2(\partial E_{01}/\partial D)(\partial E_{01}/\partial E) C_{DE}, \tag{B6}$$

where C_{ij} are just elements of the covariance matrix. The covariance matrix for sample UT1 is

$$C = \begin{pmatrix} 0.03522 & 0.01859 & 0.00168 \\ 0.01859 & 0.00991 & 0.00087 \\ 0.00168 & 0.00087 & 0.00009 \end{pmatrix} \tag{B7}$$

which gives

$$E_{01} = 2.2 \pm 0.2\ \text{cm}^{-1} \tag{B8}$$

for the splitting of the lowest pair of energy levels at zero field.

We thank E. Abresch for his help in the preparation of the reaction centers, R. Isaacson for taking the EPR spectra, Z. Fisk and B. Ricks for their assistance with the magnetometer, and P. Debrunner for helpful discussions.

The work was supported by National Science Foundation grants DMR 77-14659 and PCM 78-13699 and National Institutes of Health grant GM 13191.

Received for publication 28 May 1980 and in revised form 24 July 1980.

REFERENCES

ABRAGAM, A., and B. BLEANEY. 1970. Electron paramagnetic resonance of transition metal ions. Clarendon Press, Oxford. Chs. 3 and 7.

BARTSCH, R. G. 1971. Cytochromes: bacterial. *Methods Enzymol.* **23**:344–363.

BEVINGTON, P. R. 1969. Data reduction and error analysis for the physical sciences. McGraw-Hill, New York, Ch. 10.

BLANKENSHIP, R. E., and W. W. PARSON. 1979. The involvement of iron and ubiquinone in electron transfer reactions mediated by reaction centers from photosynthetic bacteria. *Biochim. Biophys. Acta.* **545**:424–444.

BLEIL, D. F., EDITOR. 1963. Electricity and magnetism. *In* American Institute of Physics Handbook. McGraw-Hill, New York. 5–170.

BRILL, A. S. 1977. Transition Metals in Biochemistry. Springer-Verlag, Berlin. Ch. 4, p. 100.

BUTLER, W. F. 1980. Determination of the electronic structure of Fe^{2+} in reaction centers from *Rhodopseudomonas sphaeroides* by magnetic measurements. Ph.D. Thesis. University of California, San Diego.

BUTLER, W. F., D. C. JOHNSTON, M. Y. OKAMURA, H. B. SHORE, and G. FEHER. 1978. Magnetic properties of reaction centers from *R. sphaeroides* R-26. *Biophys. J.* **21**:8 *a.* (Abstr.).

CARLIN, R. L., and A. J. VAN DUYNEVELDT. 1977. Magnetic Properties of Transition Metal Compounds. Springer-Verlag, New York. Ch. 1.

CHAMPION, P. M., and A. J. SIEVERS. 1977. Far infrared magnetic resonance in $FeSiF_6 \cdot 6H_2O$ and $Fe(SPh)_4^{2-}$. *J. Chem. Phys.* **66**:1819–1825.

CHAMPION, P. M., and A. J. SIEVERS. 1980. Far infrared magnetic resonance of deoxyhemoglobin. *J. Chem. Phys.* **72**:1569–1582.

CLAYTON, R. K., and W. R. SISTROM, EDITORS. 1978. The Photosynthetic Bacteria. Plenum Press, New York.

COFFMAN, R. E., and G. R. BUETTNER. 1979. A limit function for long-range ferromagnetic and antiferromagnetic superexchange. *J. Phys. Chem.* **83**:2387–2392.

COOKE, A. H., H. MEYER, W. P. WOLF, D. F. EVANS, and R. F. RICHARDS. 1954. The magnetic susceptibility of oxygen in a clathrate compound. I. *Proc. R. Soc. A Math. Phys. Sci.* **225**:112–121.

CORIO, P. L. 1966. Structure of High Resolution NMR Spectra. Academic Press, Inc., New York. Ch. 4.

DAVIS, P. J., and I. POLONSKY. 1964. Numerical interpolation, differentiation and integration. *In* Handbook of Mathematical Functions. M. Abramowitz and I. Stegun, editors. U. S. Government Printing Office. Washington, D. C. Ch. 25.

DEBRUNNER, P. G., C. E. SCHULZ, G. FEHER, and M. Y. OKAMURA. 1975. Mossbauer study of reaction centers from *R. spheroides. Biophys. Soc. Abstr.* **15**:226.

DIXON, W. J., and M. B. BROWN, EDITORS. 1979. *BMDP-79.* University of California Press, Berkeley. Ch. 14.

EADIE, W. T., D. DRIJARD, F. E. JAMES, M. ROOS, and B. SADOULET. 1971. Statistical Methods in Experimental Physics. Elsevier/North-Holland, Amsterdam. Ch. 8.

EISENBERGER, P. M., M. Y. OKAMURA, and G. FEHER. 1980. Investigation of the ferroquinone complex in reaction centers of *R. sphaeroides* R-26 by EXAFS. Presented at the Biophysical Society Meeting, June, 1980, New Orleans, La.

FEHER G. 1971. Some chemical and physical properties of a bacterial reaction center particle and its primary photochemical reactants. *Photochem. Photobiol.* **14**:373–388.

FEHER, G., and M. Y. OKAMURA. 1978. Chemical composition and properties of reaction centers. *In* The Photosynthetic Bacteria. R. K. Clayton and W. R. Sistrom, editors. Plenum Press, New York. 349–386.

FEHER, G., M. Y. OKAMURA, and J. D. MCELROY. 1972. Identification of an electron acceptor in reaction centers of *Rhodopseudomonas sphaeroides* by EPR spectroscopy. *Biochim. Biophys. Acta.* **267**:222–226.

FEHER, G., R. A. ISAACSON, J. D. MCELROY, L. C. ACKERSON, and M. Y. OKAMURA. 1974. On the question of the primary acceptor in bacterial photosynthesis: manganese substituting for iron in reaction centers of *Rhodopseudomonas sphaeroides* R-26. *Biochim. Biophys. Acta.* **368**:135–139.

FIGIS, B. N., and J. LEWIS. 1960. The magnetochemistry of complex compounds. *In* Modern Coordination Chemistry. Interscience Publishers Inc. John Wiley & Sons, New York. 400–454.

HUYNH, H., G. C. PAPAEFTHYMION, C.-S. YEN, J. L. GROVES, and C. S. WU. 1974. Electronic structure of Fe^{2+} in normal human hemoglobin and its isolated subunits. *J. Chem. Phys.* **61**:3750–3758.

JENNRICH, R. J., and M. L. RALSTON. 1979. Fitting nonlinear models to data. *Ann. Rev. Biophys. Bioeng.*

KESSEL, S. L., R. M. EMBERSON, P. G. DEBRUNNER, and D. N. HENDRICKSON. 1980. Iron (III), manganese (III), and cobalt (III) complexes with single chelating *O*-semiquinone ligands. *Inorg. Chem.* **19**:1170–1178.

LEFEBVRE, R., and J. MARUANI. 1965. Use of computer programs in the interpretation of electron paramagnetic resonance spectra of dilute radicals in amorphous solid samples. I. High field treatment. X-Band spectra of π electron unconjugated hydrocarbon radicals. *J. Chem. Phys.* **42**:1480–1496.

LOACH, P. A., and R. L. HALL. 1972. The question of the primary electron acceptor in bacterial photosynthesis. *Proc. Natl. Acad. Sci.* U.S.A. **69**:786–790.

LOVENBERG, W., EDITOR. 1973. The Iron Sulfur Proteins. Vols. 1 and 2. Academic Press, Inc., New York.

LOVENBERG, W. EDITOR. 1977. The Iron Sulfur Proteins. Vol. 3. Academic Press, Inc., New York.

MCELROY, J. D., G. FEHER, and D. MAUZERALL. 1970. Observation of a second light induced EPR signal from reaction centers of photosynthetic bacteria. *Biophys. Soc. Abstr.* **10**:204 *a.* (Abstr.).

McELROY, J. D., D. C. MAUZERALL, and G. FEHER. 1974. Characterization of primary reactants in bacterial photosynthesis. II. Kinetic studies of the light induced EPR signal (g = 2.0026) and the optical absorbance changes at cryogenic temperatures. *Biochim. Biophys. Acta.* **333**:261–278.

MEYER, H., M. C. M. O'BRIEN, and J. H. VAN VLECK. 1957. The magnetic susceptibility of oxygen in a clathrate compound II. *Proc. R. Soc. A Math. Phys. Sci.* **243**:414–421.

OKAMURA, M. Y., L. A. STEINER, and G. FEHER. 1974. Characterization of reaction centers from photosynthetic bacteria. I. Subunit structure of the protein mediating the primary photochemistry in *Rhodopseudomonas sphaeroides* R-26. *Biochemistry.* **13**:1394–1403.

OKAMURA, M. Y., R. A. ISAACSON, and G. FEHER. 1975. Primary acceptor in bacterial photosynthesis: obligatory role of ubiquinone in photoactive reaction centers of *Rhodopseudomonas sphaeroides. Proc. Natl. Acad. Sci. U.S.A.* **72**:3491–3495.

OKAMURA, M. Y., R. A. ISAACSON, and G. FEHER. 1978. EPR signals from the primary and secondary quinone in reaction centers of *R. sphaeroides* R-26. *Biophys. J.* **21**:8 *a.* (Abstr.).

ORGEL, L. E. 1966. An Introduction to Transition Metal Chemistry: Ligand Field Theory. Methuen, London. Ch. 3.

PARSON, W. W. 1968. The role of P_{870} in bacterial photosynthesis. *Biochim. Biophys. Acta.* **153**:248–259.

PARSON, W. W. 1978. Quinones as secondary acceptors. *In* The Photosynthetic Bacteria. R. K. Clayton and W. R. Sistrom, editors. Plenum Press, New York. 455–469.

PARSON, W. W., and G. D. CASE. 1970. In *Chromatium,* a single photochemical reaction center oxidizes both cytochrome C_{552} and cytochrome C_{555}. *Biochim. Biophys. Acta.* **205**:232–245.

PRYCE, M. H. L. 1950. A modified perturbation procedure for a problem in paramagnetism. *Proc. Phys. Soc. (London)* **63**:25–29.

PUMPHREY, A. M., and E. R. REDFEARN. 1966. A method for determining the concentration of ubiquinone in mitochondrial preparations. *Biochem. J.* **76**:61–69.

SMITH, B. T., J. M. BOYLE, J. J. DONGARRA, B. S. GARBOW, Y. IKEBE, V. C. KLEMA, and C. B. MOLER. 1976. Matrix Eigensystem Routines—EISPACK Guide. Springer-Verlag, New York.

STRALEY, S. C., W. W. PARSON, D. C. MAUZERALL, and R. K. CLAYTON. 1973. Pigment content and molar extinction coefficients of photochemical reaction centers from *Rhodopseudomonas sphaeroides. Biochim. Biophys. Acta.* **305**:597–609.

TAKAMIYA, K., and A. TAKAMIYA. 1969. Light-induced reactions of ubiquinone in photosynthetic bacterium, *Chromatium* D. III. Oxidation-reduction state of ubiquinone in intact cells of *Chromatium* D. *Plant Cell Physiol.* **10**:363–373.

VAN VLECK, J. H. 1932. The Theory of Electric and Magnetic Susceptibilities. Oxford University Press, London.

WOHLLEBEN, D., and M. B. MAPLE. 1971. Application of the Faraday method to magnetic measurements under pressure. *Rev. Sci. Instrumen.* **42**:1573–1578.

WRAIGHT, C. 1978 *a.* The role of Fe and H^+ in the quinone acceptor complex of photosynthetic reaction centers. *Biophys. J.* **21**:8 *a.* (Abstr.).

WRAIGHT, C. 1978 *b.* Iron-quinone interactions in the electron acceptor region of bacterial photosynthetic reaction centers. *FEBS Lett.* **93**:283–288.